Materials Science & Engineering A 637 (2015) 162–169

Contents lists available at ScienceDirect

Materials Science & Engineering A

journal homepage: www.elsevier.com/locate/msea

Microstructural influences on strengthening in a naturally aged and overaged Al–Cu–Li–Mg based alloy

Henry Ovri [a,*], Eric A. Jägle [b], Andreas Stark [c], Erica T. Lilleodden [a]

[a] Helmholtz Zentrum Geesthacht, Institute of Materials Research, Materials Mechanics, 21502 Geesthacht, Germany
[b] Max-Planck-Institut für Eisenforschung GmbH, Department of Microstructure Physics and Alloy Design, 40237 Düsseldorf, Germany
[c] Helmholtz Zentrum Geesthacht, Institute of Materials Research, Materials Physics, 21502 Geesthacht, Germany

ARTICLE INFO

Article history:
Received 19 January 2015
Received in revised form
5 March 2015
Accepted 15 April 2015
Available online 23 April 2015

Keywords:
TEM
APT
Al–Li–Cu alloys
Precipitates
Strengthening mechanisms

ABSTRACT

A combination of transmission electron microscopy, atom probe tomography and high-energy X-ray diffraction was employed to investigate the influence of local microstructural changes on strengthening in a commercial Al–Cu–Li–Mg based alloy, AA2198, in the stretched and naturally aged, and overaged states. Strengthening in the stretched and naturally aged temper was shown to be governed by a combination of Cu–Cu clusters, δ′/β′ phase and solution strengthening. This is in contrast to another report which suggests that strength in this temper is only due to Cu-rich clusters [B. Decreus, et al., Acta Mater., 61 (2013) 2207]. On the other hand, although large volume fractions of equilibrium phases such as T_B, and θ were present in the overaged temper, its strengthening was largely governed by order hardening, which is the strengthening mechanism associated with the δ′/β′ phase. The δ′/β′ phase remained in the matrix even after extensive overaging.

1. Introduction

Al–Cu–Li–Mg based alloys of the latest generation exhibit an excellent combination of low density, high elastic modulus and high specific strength, which makes them candidate structural materials for next generation aerospace applications [1–4]. The attractive properties of these alloys are associated with the addition of Li which not only results in significant weight reduction but also enables the formation of several strengthening precipitates including δ′ (Al_3Li), δ (AlLi), T_1 (Al_2CuLi), T_2 (Al_5CuLi_3) and T_B (Al_7Cu_4Li). Other precipitates that have been reported in these alloys include GP zones, θ′ (Al_2Cu), θ (Al_2Cu), Ω (Al_2Cu), S′ (Al_2CuMg), and β′ (Al_3Zr) [3–8]. The concentration and thermomechanical treatment given to a particular alloy dictates which of these precipitates forms in the alloy and ultimately determines its properties.

Recent studies of Al–Cu–Li–Mg-based alloy systems have focussed on AA2198 [9-12] which has shown an outstanding combination of static strength and damage tolerance along with good weldability and is therefore envisaged as a replacement for the AA2024/AA7475 alloys presently used in fuselage skin applications in commercial aircrafts [13,14]. Although the peak aged (PA) temper of this alloy is of application interest, detailed investigation of the structure–property relationships of other temper states is required since it provides the basis for understanding the influence of process-induced microstructural changes on the post-processing properties of the alloy. For instance, it was shown that the T_1 precipitate, which is the main strengthening phase in the PA temper [1,12], dissolves, while T_B phase precipitates within the grain interior and in grain boundaries during friction stir welding of peak aged AA2198 [15]. The T_B phase is an equilibrium phase that occurs only in the overaged temper of Al–Li based alloy systems [8]. It was also shown elsewhere [16] that Portevin–Le Chatelier (PLC) type plastic instability, a phenomenon associated with strain localisation and reduction in ductility [17], occurs in the overaged (OA) temper of this alloy. This phenomenon refers to continuous yielding that occurs during plastic deformation, i.e. prior to necking and it manifests macroscopically as serrations (stress drops) in the plastic region of stress–strain curves. This is in addition to the significant reduction in strength that accompanies overaging. Similarly, it was recently concluded that the stretched and naturally aged (NA) temper of AA2198 must be strengthened by Cu-rich clusters, since no precipitates were observed in selected area diffraction (SAD) or dark field (DF) transmission electron microscope (TEM) micrographs [1]. It is not clear from these studies if these clusters are associated with Mg or Li. Cu–Mg co-clusters form easily during room temperature ageing of a number of Al–Cu–Mg–(Li) alloy systems and are known to confer significant strengthening [18,19]. 1st nearest neighbour distribution (1NN) analysis of atom probe tomography (APT) data of this temper state revealed only a slight deviation from the random distribution of Cu in the matrix [20]. Whether such minor deviations can sufficiently

* Corresponding author. Tel.: +49 4152 872607; fax: +49 4152 872625.
E-mail address: henry.ovri@hzg.de (H. Ovri).

http://dx.doi.org/10.1016/j.msea.2015.04.039
0921-5093/

account for the remarkably high strength observed in this temper is an open question.

In this paper, we present a detailed study of the microstructure–property relationship of an AA2198 alloy in the stretched and naturally aged (NA) and overaged (OA) states where the T_1 phase is absent. A systematic approach involving TEM methods, high-energy X-ray diffraction (HEXRD) and APT was adopted.

2. Materials and methods

The nominal composition of the AA2198 alloy used in the present study is given in Table 1. The alloy was received in the T351 state, that is, it had been solution treated, water quenched, stretched to a strain of 2% and naturally aged for several months. The as-received temper is hereafter referred to as NA. An artificial aging protocol aimed at achieving the overaged state (OA) within a reasonable ageing time was established on the basis of the time–temperature–precipitation diagrams proposed by Chen and Bhat [21] for a similar alloy, AA2195. The protocol comprised aging at 370 °C for 10 h.

The mechanical response of the investigated tempers was determined from tensile tests conducted at a strain rate of 5×10^{-5}/s in a Zwick universal testing station equipped with a non-contact extensometer. Dog-bone shaped samples with gauge length of 11 mm and thickness of 0.6 mm, produced by wire-cut electro-discharge machining, were used in the tensile tests.

Microstructural characterisation was conducted in large part through TEM analysis using a Philips CM200 TEM and a JEOL 3010 microscope operated at 200 kV and 300 kV, respectively. A set of the TEM samples used in the analysis was prepared by electropolishing in a twin-jet device with a solution of 67% methanol and 33% nitric acid at a temperature of −20 °C and current of 12 V, while another set was produced by focused ion beam (FIB) milling in a Nova 200 Nanolab dual-beam scanning electron microscope (SEM) from FEI, Co. The thickness of the FIB-milled lamellae was measured in the SEM prior to examination in the TEM and used as the basis for determining the average volume fraction of the δ′/β′ phase. The reported volume fraction of the δ′/β′ phase is the average estimated from three different micrographs, while its precipitate size is the average of over 180 precipitates imaged in a series of micrographs.

Complementary microstructural characterisation using high-energy x-ray diffraction (HEXRD) was carried out at the HZG beamline HEMS at the Deutsches Electronen-Synchrotron (DESY) in Hamburg, Germany [22]. Samples with height of 4 mm were measured in transmission using a beam cross section of 1 mm × 1 mm. The samples were penetrated with high-energy X-rays with a photon energy of 100 keV, which corresponds to a wavelength, λ, of 0.124 Å. The resulting Debye–Scherrer diffraction rings were recorded on a 2-dimensional Perkin Elmer XRD 1622 detector with an exposure time of 0.1 s. In order to reduce background noise, 40 images were summed up for each sample, such that even weak peaks from phases with minor phase fractions were made visible. Conventional diffraction patterns were generated from the rings by azimuthal integration of the rings. Qualitative phase analysis was achieved by means of simulated diffraction patterns. The lattice parameter of the aluminium phase was determined by the Gaussian fitting method.

Quantitative elemental analysis of the matrix phase and clustering therein was carried out with a LEAP 3000X HR, local electrode atom probe operating in laser mode. The specimen temperature was set to 60 K, the laser pulse energy was 0.6 nJ, the laser pulse repetition rate varied between 100 and 250 kHz, and the target evaporation rate was set to 1% [23]. The specimens were produced by a standard lift-out procedure [24] in the Nova 200 Nanolab dual beam SEM mentioned above. The final annular milling was carried out at an accelerating voltage of 5 kV and a beam current of 70 pA. Nevertheless, some Ga contamination was detected in the APT datasets, but the corresponding peaks in the mass spectrum were ignored in the concentration and cluster analysis. There were also unusually intense peaks corresponding to AlH^+ and AlH_2^+ in the mass spectrum. This impedes the correct determination of the Si concentration, because both AlH^+ and $^{28}Si^+$, and AlH_2^+ and $^{29}Si^+$ have mass-to-charge ratios of 28 and 29, respectively. In this study, the peak at 28 Da was assigned to Si while that at 29 Da was assigned to AlH_2. 3D reconstruction was performed in the software IVAS (version 3.6.8) by Cameca using the initial tip apex radii and shank angles as determined by SEM before the experiments. Cluster analysis was performed in the software 3Depict (version 0.0.17) using the core-link algorithm. The cluster analysis parameters were determined according to the heuristic method used by Marceau [25].

Table 1
Overall matrix concentration of the naturally aged (NA) and overaged (OA) tempers as measured from APT experiments. The concentration range given by the manufacturer (nominal) is also included in the table.

Element at%	Li	Cu	Mg	Ag	Zr	Si
Nominal	3.11–4.27	1.23–1.48	0.29–0.80	0.03–0.12	0.01–0.05	0.08
NA	3.24	1.10	0.26	0.15	–	0.28
OA	3.14	0.40	0.26	0.04	–	0.18

3. Results

3.1. Tensile test

Fig. 1 shows the true stress, σ_t, vs. true strain, ε_t, response of each temper. The NA temper exhibited remarkably high yield strength, 310 MPa, about a factor of three higher than in the OA temper. PLC type – plastic instability was also observed in the OA temper. A portion of the σ_t, vs. ε_t curve of the OA temper is magnified in the inset in Fig. 1 to more clearly reveal the stress drops associated with the plastic instability. It is noteworthy that the NA temper sustained a higher plastic strain than the OA temper even though its yield strength is about a factor of 3 higher than the latter. This observation underscores the detrimental effect of plastic instability on ductility. A plot of the work hardening rate ($d\sigma_t/d\varepsilon_t$) as a function of true strain is also superimposed on Fig. 1. The very early stage of plastic deformation in the OA tempers showed significantly higher work hardening rate in comparison to the NA temper. The high work hardening rate of the OA temper however decreased rapidly, after

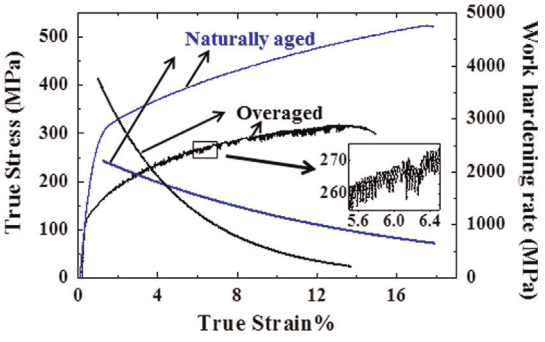

Fig. 1. (a) True stress–true strain response of AA2198 in the naturally aged (NA), in blue, and overaged (OA), in black, temper states. Plastic instabilities are observed in the overaged temper. (b) Work hardening rates ($d\sigma_t/d\varepsilon_t$) of each temper plotted as a function of true plastic strain. (For interpretation of the references to colour in this figure legend, the reader is referred to the web version of this article.)